PHOTOMETRY OF VARIABLE STARS FROM DOME A, ANTARCTICA: RESULTS FROM THE 2010 OBSERVING SEASON

Lingzhi Wang[1,2,3,4], Lucas M. Macri,[2] Lifan Wang[2,3,5], Michael C. B. Ashley[6],
Xiangqun Cui[3,7], Long-Long Feng[3,5], Xuefei Gong[3,7], Jon S. Lawrence[6,8], Qiang Liu[3,4],
Daniel Luong-Van[6], Carl R. Pennypacker[9], Zhaohui Shang[3,10], John W. V. Storey[6],
Huigen Yang[3,11], Ji Yang[3,5], Xiangyan Yuan[3,7], Donald G. York[12], Xu Zhou[3,4],
Zhenxi Zhu[3,5] & Zonghong Zhu[1,3]
Accepted for publication in the Astronomical Journal

ABSTRACT

We present results from a season of observations with the Chinese Small Telescope ARray (CSTAR), obtained over 183 days of the 2010 Antarctic winter. We carried out high-cadence time-series aperture photometry of 9,125 stars with $i \lesssim 15.3$ mag located in a 23 square-degree region centered on the south celestial pole.

We identified 188 variable stars, including 67 new objects relative to our 2008 observations, thanks to broader synoptic coverage, a deeper magnitude limit and a larger field of view.

We used the photometric data set to derive site statistics from Dome A. Based on two years of observations, we find that extinction due to clouds at this site is less than 0.1 and 0.4 mag during 45% and 75% of the dark time, respectively.

Subject headings: site testing – stars: variable: general

1. INTRODUCTION

Synoptic (time-series) astronomy has undergone a dramatic transformation over the past decade thanks to advances in imaging and computer technology. Many high-impact discoveries have taken place, such as transiting exoplanets (Charbonneau et al. 2000) and the detection of supernovae mere hours after explosion (Nugent et al. 2011). These and other astrophysical problems benefit from long, continuous and stable time-series photometry, which until recently could only be achieved from space or via coordinated observations by a world-wide telescope network. The former alternative is expensive, while the latter is fraught with calibration issues, variable weather across the sites, and is highly labor intensive.

One region on Earth – the Antarctic Plateau – offers an excellent alternative to the aforementioned options by providing a combination of extended periods of dark time, high altitude, low precipitable water vapor, extremely low temperatures and a very stable atmosphere

with greatly reduced scintillation noise (Kenyon et al. 2006). These conditions enable new or extended observation windows in the infrared and sub-milimeter regions of the electromagnetic spectrum, as well as improved conditions at optical and other wavelengths. The resulting gains in sensitivity and photometric precision over the best temperate sites can reach several orders of magnitude (Storey 2005, 2007, 2009; see also Tables 2 & 4 and Figures 7-11 in Burton 2010). The long "winter night" that occurs at these latitudes and the minimal daily change in elevation for any given source make the performance of a polar site equivalent to that of a six-site network at temperate latitudes (Mosser & Aristidi 2007). Some disadvantages include the reduced fraction of the celestial sphere that can be observed, prolonged twilight, and possibility of aurorae.

According to metereological studies carried out by Saunders et al. (2009, 2010), the region surrounding Dome A (elevation: 4,093 meters above mean sea level) in the Antarctic plateau is likely the best astronomical site on Earth. In order to further investigate the conditions at this promising site, we developed an observatory capable of year-round operations called PLATO (Ashley et al. 2010; Luong-Van et al. 2010; Yang et al. 2009; Lawrence et al. 2009; Lawrence et al. 2008; Hengst et al. 2008; Lawrence et al. 2006), and a quad-telescope called CSTAR (the Chinese Small Telescope ARray, Yuan et al. 2008; Zhou et al. 2010b). The observatory is part of the Chinese Kunlun station, located at Dome A.

Several papers were written based on a large amount of high-quality photometric data obtained during the 2008 Antarctic winter: Zou et al. (2010) undertook a variety of sky brightness, transparency and photometric monitoring observations; Zhou et al. (2010a) published a photometric catalog of $\sim 10,000$ stars; and Wang et al. (2011) presented the first catalog of variable stars in the CSTAR field of view.

[1] Department of Astronomy, Beijing Normal University, Beijing, China
[2] Mitchell Institute for Fundamental Physics & Astronomy, Department of Physics & Astronomy, Texas A&M University, College Station, TX, USA
[3] Chinese Center for Antarctic Astronomy, Nanjing, China
[4] National Astronomical Observatory of China, Chinese Academy of Sciences, Beijing, China
[5] Purple Mountain Observatory, Chinese Academy of Sciences, Nanjing, China
[6] School of Physics, University of New South Wales, NSW, Australia
[7] Nanjing Institute of Astronomical Optics and Technology, Nanjing, China
[8] Australian Astronomical Observatory, NSW, Australia
[9] Center for Astrophysics, Lawrence Berkeley National Laboratory, Berkeley, CA, USA
[10] Tianjin Normal University, Tianjin, China
[11] Polar Research Institute of China, Pudong, Shanghai, China
[12] Department of Astronomy and Astrophysics and Enrico Fermi Institute, University of Chicago, Chicago, IL, USA
Current email address: wanglingzhi@bao.ac.cn

This paper presents an analysis of the data acquired by the CSTAR#3 telescope during the 2010 Antarctic winter season. §2 briefly describes the observations and data reduction; §3 describes the steps followed to obtain high-precision time-series photometry of the brightest 9,125 stars with well-sampled light curves; §4 discusses the variable stars we discovered and §5 contains our conclusions.

2. OBSERVATIONS AND DATA REDUCTION

2.1. *Observations*

Observations were carried out using the same CSTAR telescope (unit #3) which we described in detail in Wang et al. (2011). Briefly, it is a Schmidt-Cassegrain wide-field telescope with a pupil entrance aperture of 145 mm, a Sloan i-band filter, and a $1K \times 1K$ frame-transfer CCD with a plate scale of $15.7''/$ pix, giving a field of view $4.5°$ on a side. The telescope and camera have no moving parts, to allow for robust operation in the extreme conditions of the Antarctic winter. Therefore, the field of view is centered on the South Celestial Pole (SCP), which lies $\sim 9°$ from the zenith at this site, and exposures are short (20-40s) to prevent star trails. The SCP field probes the inner halo of the Milky Way ($l = 303°, b = -27°$) and has moderate extinction ($A_i = 0.31$ mag, Schlafly & Finkbeiner 2011).

Scientifically-useful images were acquired from 2010 March 29 to 2010 September 27. Table 1 lists the number of images and total integration time per month and Table 2 lists the different integration times used throughout the observing season. More than 338,000 images (equivalent to over 360 GB of data) were collected with a total integration time of 2,553 hours.

2.2. *Data Reduction*

The preliminary data reduction for raw science frames involved bias subtraction, flat fielding, correction for variations in sky background, fringe pattern subtraction and bad pixel masking. We used the same bias frame from our previous paper, which was created during instrument testing in China. We generated a sky flat by median-combining 2,700 frames with high sky level ($>$ 10,000 ADU) taken throughout the observing season during twilight conditions (Sun elevation angle between 0 and $-10°$). Prior to combining the images, we masked any stars present in the individual frames using a detection threshold of 2σ, as well as regions within 10 pixels of any pixel close to saturation (defined as $>25,000$ ADU).

Approximately 35% of the bias-subtracted and flatfielded images showed low-frequency sky background variations with an amplitude of $\sim 3\%$ of the mean value, which we subtracted by the following method. We divided each image into 1,024 square sections (32 pixels on a side) and computed the mean and standard deviation of the sky value in each section using the procedure implemented in DAOPHOT (Stetson 1987). We did not use any sections with sky values above 20,000 or below 0 ADU, or those with standard deviations that exceeded 300 ADU. Those properties are typical of very crowded regions of an image, or indicate the presence of a very bright star, so we replaced the sky value of those sections with the median value of their nearest ten neighbors. We

TABLE 1
LOG OF OBSERVATIONS

Month 2010	# images	Total exp. time (hr)
March	1587	17.6
April	31110	345.7
May	39651	405.8
June	69509	579.2
July	97310	631.1
August	73088	406.0
September	30098	167.2
Total	**342353**	**2552.6**

TABLE 2
EXPOSURE TIMES

Start date	End date	Exp. (s)	# images
2010-03-29	2010-05-26	40	59843
2010-05-26	2010-07-13	30	114577
2010-07-13	2010-09-27	20	167933

generated a full-resolution background model frame by fitting the 1,024 sky values using a thin-plate spline. We calculated the standard deviation of sky values before and after model subtraction; if the reduction in the scatter was less than a factor of 2, we reduced the section size to 16 pixels on a side and repeated the procedure.

The background-subtracted images exhibited a fringe pattern, which is commonly encountered in CCD images obtained at near-infrared wavelengths (for a review, see Howell 2012). We created a fringe correction frame and removed this instrumental signature from our images following these steps. First, we selected 1,500 images taken each month with the lowest sky levels during dark time (Sun elevation angle below $-18°$) and 1,500 images taken during twilight. This yielded 7 sets of images obtained during twilight and 5 sets acquired during dark time (April to August). The motivation behind creating the two different sets was to check for variations in fringe amplitude as a function of Sun elevation angle.

Next, we removed stars by masking any pixel lying more than 2σ above the sky level. We combined the frames in each of the 12 sets by sorting the un-masked pixels at each (x, y) position, discarding the lowest 10 values (where the fringe pattern was too low to be useful), and averaging the next 50 values. The fringe pattern had an average peak-to-peak amplitude of 2% of the mean sky value, with no statistically significant variation as a function of time or Sun elevation angle. Therefore, we generated the final fringe frame by taking the minimum pixel value at each location among the 12 sets (to further ensure that no stellar sources were included). The fringe pattern was subtracted from individual frames by iteratively scaling the correction image until the sky background exhibited the lowest *r.m.s.* value.

3. PHOTOMETRY

3.1. *Frame Selection and Photometry*

We carried out initial photometric measurements on the debiased, flattened, sky-subtracted and fringe-corrected images using the same pipeline and procedures
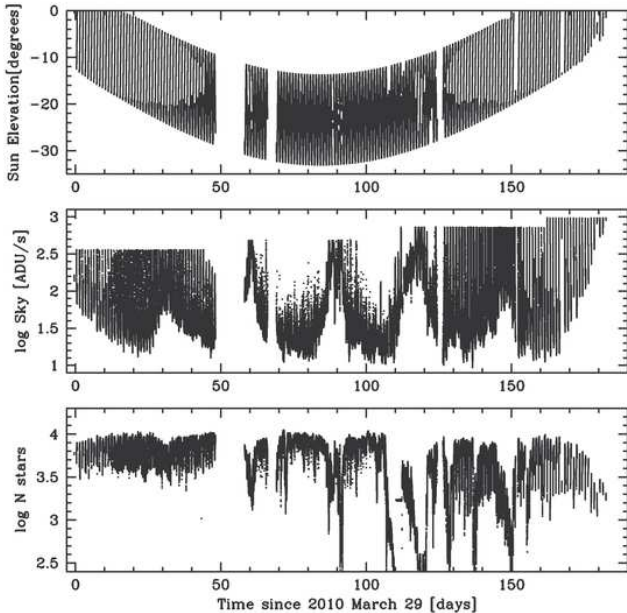
FIG. 1.— Time-series plots of Sun elevation angle (top panel), sky brightness level (middle panel), and number of stars detected in each image (bottom panel).

FIG. 2.— Comparison of the mean instrumental magnitudes of bright stars in common between the 2008 and 2010 CSTAR observations.

described in Wang et al. (2011), which we briefly summarize here. Given the extremely undersampled nature of the images, we performed aperture photometry using DAOPHOT Stetson (1987). We set the aperture radius to 2.5 pixels (equivalent to $39.3''$) and the sky annulus extended from 4 to 7 pixels (equivalent to $62.8 - 109.9''$). The detection threshold was set to 5σ above the sky background, which typically corresponded to $i \sim 14$ mag.

Figure 1 displays the Sun elevation angle (top panel), sky background in ADU s^{-1} (middle panel), and number of stars detected (bottom panel) for each image as a function of time since 2010 March 29. The sky background shows a clear monthly pattern related to the lunar phase. During most of the winter season, the data acquisition system was programmed to stop when the sky level exceeded 14,600 ADU; this limit was raised to 19,400 after 2010 Sep 7. We initially selected frames with Sun elevation angle below $0°$ and more than 1,500 stars. These criteria were met by 85.5% (289,343) of all the images acquired during the Antarctic winter. A period of bad weather and ice buildup on the top cover of the instrument during the month of July resulted in the rejection of $\sim 35,000$ images (equivalent to 8 days of operations).

The selected images have a median sky level of 32 ADU s^{-1}, equivalent to a median sky background of $i = 19.8$ mag/$\square''$. This value is identical to the value derived by Zou et al. (2010) and similar to our previous determination of 19.6 mag/$\square''$ (Wang et al. 2011). Note that all these estimates include contributions from moonlight. The darkest sky background measured during the season (on clear moonless nights) was $i \sim 20.9$ mag/$\square''$. The median value of the number of stars detected in an individual frame is 8,600, higher than the corresponding value of 7,500 from the 2008 observations. We attribute this increase to the subtraction of sky background variations described in § 2.2, which enabled the detection of
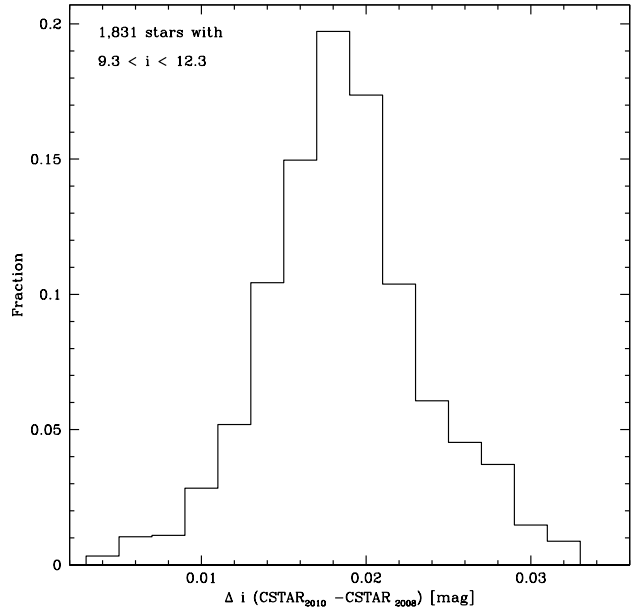
fainter stars at a fixed threshold.

We used the initial photometry to register all frames using DAOMATCH and DAOMASTER and created a reference image (hereafter, "master frame") with $4\times$ finer spatial sampling. We followed the same procedure described in our previous paper, this time based on 2,580 high-quality images obtained during 2010 June 13. We carried out aperture photometry on the master frame using the same parameters listed above and detected approximately 155,000 stars, reaching a depth of $i \sim 20.9$ mag. Additionally, we performed point-spread function photometry that, despite its lower quality due to the undersampled nature of the images, enabled us to estimate the relative magnitudes of stars with overlapping apertures.

3.2. Photometric corrections

We performed all the photometric corrections described in detail in Wang et al. (2011), which included: exposure time normalization, zeropoint correction, sigma rescaling, residual flat fielding, time calibration, masking of satellite trails and saturated regions, spike filtering, and magnitude calibration. We will only discuss the details of magnitude and time calibration since the rest of the procedures were identical to our previous work.

We performed the magnitude calibration by matching the mean instrumental magnitudes of 1,831 stars with $9.3 \leq i \leq 12.3$ mag in common between our 2010 and 2008 master frames. Since the mean instrumental magnitudes of each season are referenced to individual images obtained under the best observing conditions (in terms of sky background and number of stars) we would expect them to reflect photometric conditions and therefore have very similar zeropoints. Indeed, we found a zeropoint offset of only 0.018 ± 0.005 mag as shown in Fig. 2. We transformed the instrumental magnitudes to
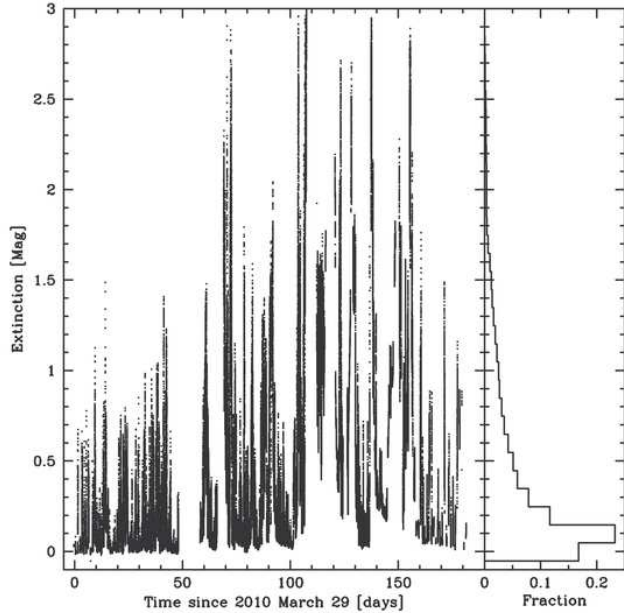
Fig. 3.— Left panel: time series plots of differential extinction, right panel: distribution of differential extinction.

Fig. 4.— Drift between true local time and computer time, fitted by two fourth-order polynomials.

the Sloan photometric system by applying the offset of 7.45 ± 0.04 mag previously derived in §3.2 of Wang et al. (2011). That offset was based on the comparison of our photometry with the i synthetic magnitudes derived by Ofek (2008) using the *Tycho* catalog, which carries an additional systematic uncertainty of 0.02 mag.

Figure 3 shows a time series and a histogram of differential extinction values, based on the photometry procedures described above. We find that extinction due to clouds in the i band at Dome A is less than 0.4 mag during 70% of the dark time, and less that 0.1 mag during 40% of the dark time. These values are similar to those previously derived for the 2008 Antarctic winter season (80% and 50%, respectively, from Wang et al. 2011).

The computer associated with the CSTAR#3 telescope has a GPS receiver to maintain time synchronization, and this time was to be distributed to computers controlling the other CSTAR telescopes (including the one used for these observations). However, there was a communication problem between the computers throughout the entire observation period, which led to a drift in the time stamp of the FITS images. §4.3 of Zhou et al. (2010a) contains details of the time calibration for the 2008 data; we carried out a similar procedure for the 2010 data as explained below.

We performed the time calibration in three steps. First, we identified two bright stars located very close to R.A.=0h and measured the angle (with respect to the x-axis) of a line extending from the SCP to their positions. We calculated the difference between the measured angle and the one predicted from the time in the FITS headers, and fit a fourth-order polynomial to solve for the time drift. The smallest dispersion was obtained by fitting two different polynomials for the data acquired before and after 2010 June 17. The total clock drift over 6 months amounted to ~ 190 seconds as seen in Fig. 4. Next, we used 19 entries in a log (obtained for engineering pur-
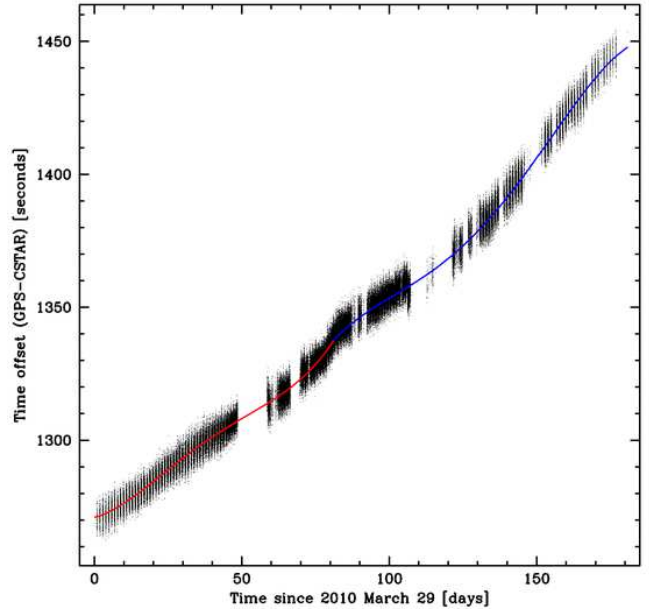
poses throughout the season) that listed the time offset between the CSTAR#3 computer and another computer at Dome A which had maintained GPS synchronization. While these data points were not sufficient to solve for the time drift, they served to transform our relative measurements into an absolute reference frame. We obtained an offset of 1337.5 ± 1.6 s. Lastly, we applied a transformation to the heliocentric reference frame.

We later checked the derived time offset by performing a cross-correlation of the light curves of 33 bright, high-amplitude, periodic variables (such as eclipsing binaries and RR Lyraes) that we had previously detected in Wang et al. (2011). We used the latest implementation of the Phase Dispersion Minimization algorithm (Stellingwerf 1978, 2011), which can robustly handle large gaps in the time series and combines all light curve "segments" to determine a common period. Using this approach, we found a consistent (but less precise) offset of 1270 ± 245 s.

4. VARIABLE STARS IN THE CSTAR FIELD

While the primary goal of CSTAR observations is to characterize the observing conditions at Dome A, the rapid cadence of image acquisition and the long duration of the winter night make this a relatively unique data set for studying variable stars and searching for extrasolar planets via the transit method. We used several complementary techniques (described below) to identify variables among the selected stars, since no single approach is sensitive to all types of stellar variability. Some of the methods we used are only sensitive to periodic variability. Most of the algorithms we used are available as part of the VARTOOLS light curve analysis program of Hartman et al. (2008).

Having already characterized the observing conditions at the site based on all the "dark time" data, we restricted our variable-star analysis to the images obtained
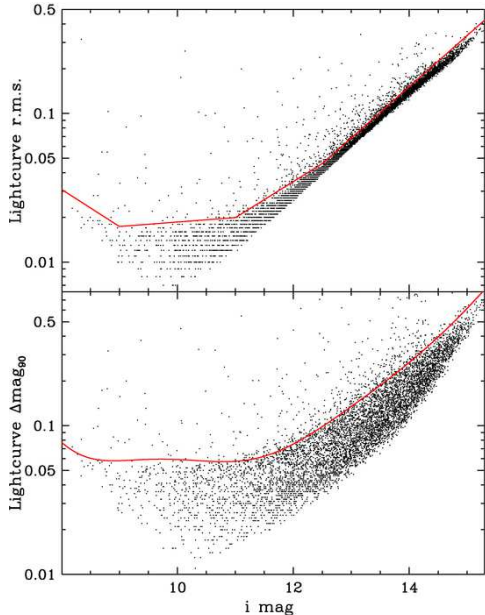
FIG. 5.— *r.m.s.* (top) and 90%-ile magnitude range (bottom) of the lightcurves of 9,125 selected stars with sufficient synoptic coverage (see text for details).

FIG. 6.— Variability statistic J (Stetson 1996) for 9,125 selected stars with sufficient synoptic coverage (see text for details).

under the best observing conditions, which we defined as a sky background below 100 ADU s^{-1} and an extinction ≤ 0.5 mag. These criteria were met by 169,500 frames (the "science-quality" sample), corresponding to about 60.9% of the previously selected set of images. Among the rejected images, 3.7% failed to provide a reliable coordinate transformation with respect to the reference frame.

We initially selected the brightest 20,000 stars in the master frame (corresponding to a depth of $i \sim 15.3$ mag) for time-series aperture photometry. Once the measurements were carried out, we restricted our analysis to 9,125 objects with valid measurements in at least 20% of the individual science-quality frames (or in 20% of all possible 3,000s time segments) in order to ensure sufficient synoptic coverage. This restriction implies a maximum declination limit of $-87°13'$ for objects in the sample, which we will later use when comparing our variable star statistics with previous studies.

We complemented the search for variables with information obtained from the PSF photometry previously carried out on the master frame, which had a 4× finer pixel scale and represented a 24-hour average stellar flux. For each object of interest, we calculated the fraction of contaminating flux contributed all other stars located closer than a certain distance: the aperture radius ($39.3''$), the inner edge of the sky annulus ($62.8''$), and the outer edge of the sky annulus ($109.9''$). We refer to these three fluxes hereafter as "close", "medium" and "far" respectively.

4.1. *Search for variability*

The first phase of our search for variable stars was aimed at identifying objects with statistically significant variations in magnitude that did not necessarily display a periodic behavior during our observations – including
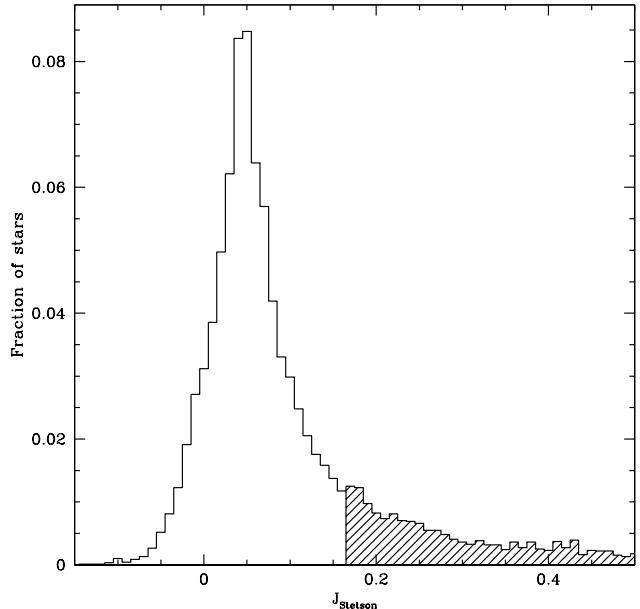
objects such as Miras, other very long-period variables and irregular variables. We used a combination of three metrics to separate constant from variable stars, as detailed below.

We calculated the *r.m.s.* and the magnitude range spanned by 90% of data points (hereafter, Δi_{90}) of the light curves of all stars. We determined upper 2σ envelopes for both quantities as a function of magnitude, shown with red lines in Fig. 5. Stars lying above both envelopes were flagged as possible variables for further analysis. The upturn in both envelopes for $i < 9$ mag is probably due to a combination of factors, including the onset of non-linearity in the detector and the dearth of truly constant stars in this magnitude range within our field. The Besançon model of the Galaxy (Robin et al. 2003) predicts that post-main sequence stars (which are very likely to exhibit variability, see Henry et al. 2000) will outnumber main-sequence objects by a ratio of 7 to 1 at this magnitude.

The lowest light curve *r.m.s.* values (7 mmag) are found at $i \sim 10$ mag, reaching within a factor of 5 of the expected scatter due to scintillation (Young 1967) for our telescope at Dome A. Given the large number of individual measurements in our photometry, bright ($i < 13.5$ mag) stars lying below both envelopes have statistical uncertainties in their mean magnitudes below 2×10^{-4} mag. As discussed in §3.2 and in Wang et al. (2011), the overall uncertainty of the photometry is dominated by the statistical (±0.04 mag) and systematic (±0.02 mag) uncertainties of the calibration procedure.

Next, we computed the Welch-Stetson variability index J (§2 of Stetson 1996), including the usual rescaling of the reported DAOPHOT magnitude errors (Udalski et al. 1994; Kaluzny et al. 1998). The result of this analysis is shown in Fig. 6; as expected for the J statistic, there is a gaussian distribution of values with a

mean value close to zero (corresponding to stars with no significant variability), and a one-sided tail (towards positive values) of candidate variable stars. We determined a mean value of $J = 0.049 \pm 0.038$ by fitting a Gaussian function to all objects with $|J| < 0.3$, and flagged stars with $J \geq 0.164$ (equivalent to a $+3\sigma$ selection) for further inspection.

We combined the $r.m.s.$, Δi_{90} and J criteria listed above to select 44 variable stars. In addition to passing all 3 variability criteria, the selected objects were also restricted to have contaminating fluxes from nearby companions in the "medium" and "far" apertures below 11.5% and 23% of the total flux, respectively. These limits may have resulted in the rejection of some *bona fide* aperiodic variables or transient events, but they serve to eliminate false positives from our sample.

4.2. *Search for periodic variability*

The J statistic was designed to be sensitive to statistically significant photometric variability between neighboring data points, and is well suited to detect continuously-varying objects such as pulsating stars (Miras, Cepheids, RR Lyrae, δ Scuti, etc.) or contact binaries. It is not particularly sensitive to detached eclipsing binaries (where the variation is restricted to a very small fraction of the phase) or to objects where the variation only becomes statistically significant after phasing many cycles (such as transiting exoplanets or very low amplitude pulsators). Similarly, the other two metrics used in the first phase of the search for variables (light curve $r.m.s.$ and Δi_{90}) lack sensitivity to small-scale periodic variations. Therefore, we searched for *periodic* variability among the stars that had failed one or more of the previous selection criteria using two of the techniques described in detail in Wang et al. (2011): the Lomb-Scargle method (Lomb 1976; Scargle 1982, hereafter LS) and the "box fitting algorithm" of Kovács et al. (2002, hereafter BLS).

Given the design of the CSTAR system, stars describe daily circular tracks through the CCD. This can lead to spurious detections of periodicity due to small residual flat-field variations. Fortunately, these false positives are easily identified and discarded because the variations occur at frequencies close (0.5-3%) to 1 cycle per sidereal day and their (sub-)harmonics. We considered an object to have significant periodic variability if the period determined by VARTOOLS (based on either the LS or the BLS technique) had a SNR> 30 and lied outside of the excluded frequencies. We imposed a minimal restriction on contaminating flux for this search, removing 2% of objects where the contaminating flux from other stars in the "close" aperture exceeded 40% of the total. The search for periodic variables can tolerate substantially larger contamination from neighbors for several reasons: very close neighbors (within the instrumental PSF or the measurement aperture) can only decrease the amplitude of the variation but cannot result in a false positive, and future observations can be used to identify which of the confused stars is the actual variable; stars outside the measurement aperture but within the outer sky annulus may produce noisier measurements but the long span of our observations still yields high-quality binned light curves that satisfy the requirement on the SNR of the period determination; any companions that somehow in-

duce a spurious periodic variation will do so at frequencies of 1 cycle/day or one of its harmonics and those have already been removed from consideration.

We detected an additional 136 variables using the LS technique and a further 8 variables using the BLS technique. These algorithms were also applied to the variables previously selected in §4.1 and 16 of those objects were found to exhibit a significant periodicity. The initial periods were refined using the Period04 program (Lenz & Breger 2005) and the Phase Dispersion Minimization algorithm (Stellingwerf 1978, 2011).

Approximately two thirds of the periodic variables exhibit a highly regular variation both in terms of period and amplitude (e.g., eclipsing binaries, normal RR Lyraes), a few have a long-term modulation in amplitude (e.g., Blazhko RR Lyraes), and about one third show variations at multiple frequencies. In the latter two cases, we based our analysis in the most significant period.

4.3. *Properties of variable stars*

Table 3 lists the properties of all detected variables. Column 1 has the 2010 CSTAR ID (a letter n is added at the beginning to avoid confusion with 2008 CSTAR IDs from our previous work); column 2 lists the 2008 CSTAR ID from (Wang et al. 2011), if applicable; column 3 presents the ID from the Guide Star Catalog, version 2.3.2 (GSC2.3), when available; columns 4 and 5 give the right ascension and declination; column 6 contains the mean i-band magnitude; column 7 lists the 90% range of the i-band light curve; column 8 has the J value; column 9 lists the most significant period (when applicable); column 10 specifies the technique used to find the period; column 11 gives the first time of minimum light contained in our observations (listed only for the periodic variables); column 12 contains a tentative classification of the variable type, when possible; column 13 has additional information, including previous identification of the variables by the All-Sky Automated Survey (Pojmanski 2005, ASAS,) or inclusion in the General Catalogue of Variable Stars (GCVS, Samus et al. 2009). Representative light curves of periodic variables are shown in Fig. 7, while two-season light curves of selected long-term variables are plotted in Fig. 8. Detailed finding charts including light curve plots for all variables are available through the Chinese Virtual Observatory[14]. All light curve data is also available through this site.

We detected a total of 188 variables in the 2010 CSTAR data, consisting of 67 new objects and 121 stars in common with Wang et al. (2011). We did not recover 36 objects classified as variables in our previous paper for the following reasons: 10 did not have enough data points, 7 were blended, and 19 did not meet the selection criteria adopted in this paper. The new variables detected in this study relative to our previous work were made possible by the deeper magnitude limit and slightly larger field of view ($\delta < -87°13'$) of the 2010 observations, which were respectively due to better sky subtraction and improved alignment of the center of the field with the SCP.

Thanks to the greater depth and synoptic coverage of our observations, we obtained a $\sim 4\times$ increase in the number of variables with $\delta < -87°13'$ relative to

---

[14] `http://casdc.china-vo.org/data/cstar`

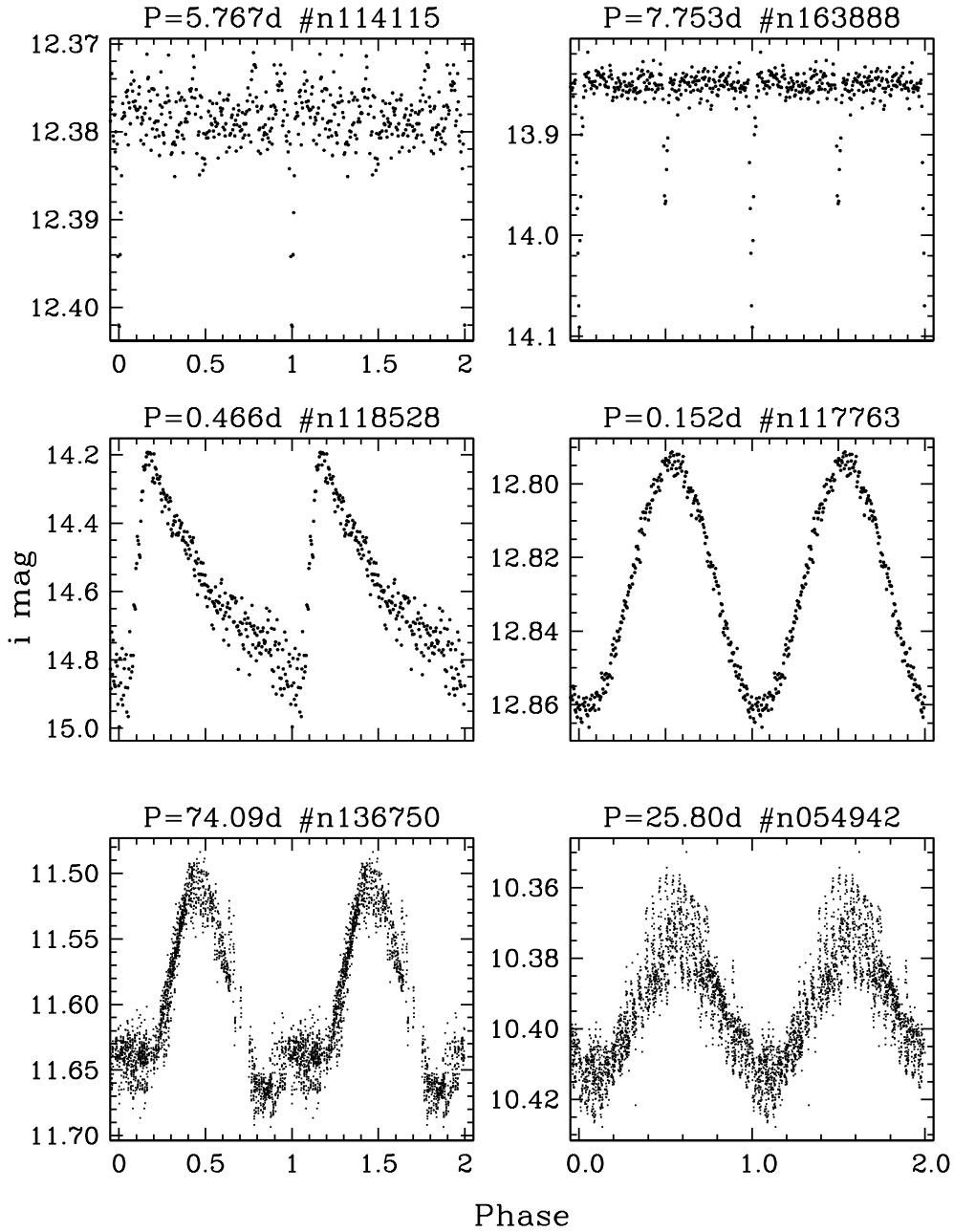FIG. 7.— Phased light curves of six newly detected periodic variable stars. The periods and 2010 CSTAR IDs are given above each panel. Top row: transiting exoplanet candidate and detached eclipsing binary; middle row: RR Lyrae and δ Scuti; bottom row: multi-periodic variables phased at the most significant period.
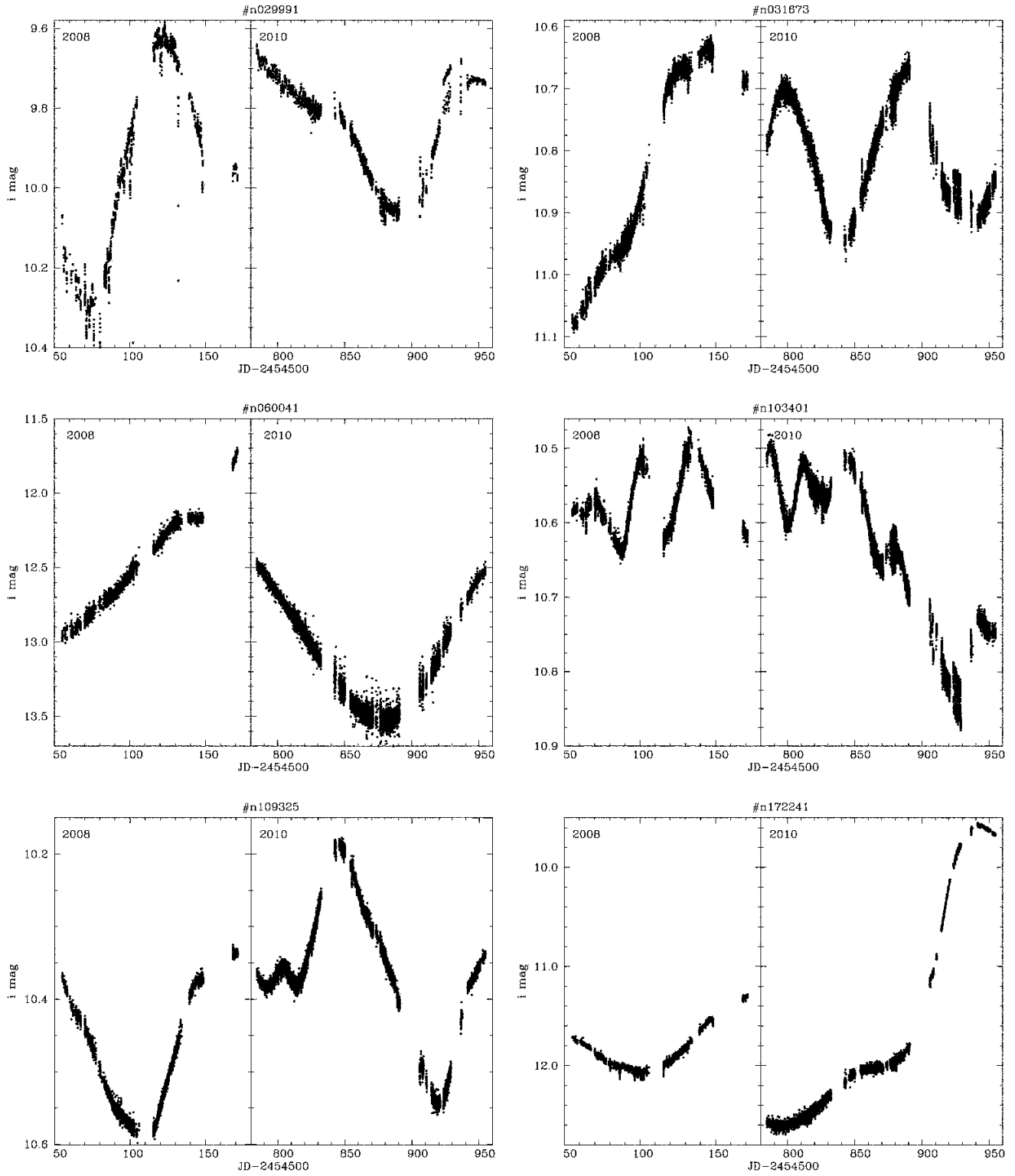
Wang et al.

FIG. 8.— Two-year light curves (left: 2008; right: 2010) for variables with long-term trends.

TABLE 3
Variable stars

	ID		R.A.	Dec.	i	Δi_{90}	J	Period		T_0^3	Class[4]	Note[5]
2010	2008	GSC	(J2000.0)[1]		(mag)			(d)	Src[2]	(d)		
n010320	. . .	S742000016	12:04:48.75	−87:23:06.0	8.79	0.18	9.68	. . .	. . .	. . .	IR	A
n012443	001707	S74D000321	12:32:42.91	−87:26:22.9	11.10	0.55	9.95	0.338544	LS	785.6824	EC	A
n012506	. . .	S3Y9000067	11:44:32.67	−87:27:35.9	10.89	0.12	2.07	31.447988	LS	. . .	MP	
n015318	003125	S3YM000469	10:43:46.63	−87:25:10.1	9.69	0.09	3.32	3.602742	LS	. . .	MP	
n015705	. . .	S3YM000358	10:04:32.92	−87:13:44.7	10.97	0.08	0.65	19.081678	LS	. . .	MP	
n016257	003697	S742000061	12:08:11.93	−87:35:39.9	11.56	0.08	0.75	26.567900	LS	. . .	MP	
n016505	003850	S742000043	12:34:25.12	−87:34:37.7	10.14	0.06	1.59	17.251594	LS	. . .	MP	A
n017573	004463	S3YM000518	10:40:16.05	−87:29:29.8	11.16	0.06	0.58	0.869262	LS	785.7941	ED	
n017781	. . .	S74D000351	13:21:24.66	−87:29:48.4	12.41	0.10	0.25	4.822329	LS	. . .	MP	
n020508	. . .	S74D000440	13:01:58.40	−87:39:56.3	9.01	0.16	3.11	5.798380	LS	786.5008	ED	
n023757	. . .	S3YM000018	09:51:32.15	−87:28:32.7	13.24	0.18	0.20	0.240900	LS	785.4140	PR	
n024696	009171	S3YM000662	10:12:54.85	−87:38:22.9	14.10	0.77	1.29	0.591726	LS	785.4091	RL	A
n025073	. . .	S3YN000420	09:29:27.99	−87:21:39.6	9.01	0.32	18.03	. . .	. . .	. . .	IR	A
n025734	009952	S742000182	12:43:30.67	−87:53:30.9	11.30	0.20	2.89	23.819339	LS	. . .	MP	A
n027942	011616	S3Y9000240	10:56:28.86	−87:55:21.0	11.97	0.08	0.55	27.282715	LS	. . .	MP	
n028073	011709	S742000246	12:41:44.27	−87:58:28.5	11.37	0.07	0.77	2.951167	LS	787.1734	PR	
n028235	011796	S742000286	12:21:35.82	−88:00:14.5	12.20	0.26	0.90	1.892910	LS	786.9435	ES	
n029044	. . .	S742000186	13:28:28.82	−87:53:09.2	9.52	0.04	1.86	11.564653	LS	. . .	MP	
n029991	013255	S74F000377	14:54:21.37	−87:21:05.0	9.87	0.34	6.41	. . .	. . .	. . .	IR	A
n030008	013140	S3Y9000236	10:25:53.99	−87:53:40.8	9.83	0.07	1.40	20.978237	LS	. . .	MP	
n031343	014111	S74F000634	14:29:01.63	−87:38:16.2	13.74	0.42	0.67	0.174082	LS	785.3263	DS	
n031673	014368	S3YM000753	10:03:10.79	−87:51:06.2	10.81	0.25	5.38	95.147196	LS	. . .	MP	
n031801	014495	S3Y9000339	10:49:00.65	−88:02:17.2	12.30	0.12	0.65	19.218473	LS	. . .	MP	
n034888	016836	S742030458	12:49:16.22	−88:11:17.6	13.74	0.30	0.47	0.176214	LS	785.2034	DS	
n035474	. . .	S74F007170	15:09:55.59	−87:25:01.9	9.09	0.08	2.89	. . .	. . .	. . .	IR	
n037305	018708	S3YN000609	09:02:20.82	−87:37:41.0	12.38	0.09	0.25	1.627880	LS	785.2541	ES	
n039537	020436	S3YN000517	08:40:33.28	−87:28:38.6	12.60	0.23	0.76	61.305131	LS	. . .	MP	
n039664	020526	S742000504	13:23:49.26	−88:16:04.3	12.46	0.42	1.53	2.510726	LS	786.9545	ES	A
n040035	. . .	S3Y9000616	11:52:51.12	−88:23:28.9	9.21	0.06	1.73	17.086312	LS	. . .	MP	
n042221	022489	S3Y9000527	10:01:21.80	−88:13:30.8	11.89	0.22	2.51	0.652314	LS	785.7043	EC	A
n043406	. . .	S3YN000632	08:39:40.85	−87:39:02.3	12.21	0.10	0.26	7.165431	BLS	787.9603	ED	
n043566	023614	S742000638	12:09:34.38	−88:29:59.0	11.49	0.05	0.32	17.256627	LS	. . .	MP	
n044666	. . .	S3Y9000612	10:32:32.73	−88:25:02.6	13.73	0.14	0.09	3.535402	BLS	788.5108	ED	
n045656	. . .	S742000672	14:20:52.04	−88:14:33.4	12.65	0.08	0.25	0.400924	LS	785.2228	EC	
n045983	025440	S742000656	12:12:56.28	−88:34:11.6	10.77	0.03	0.37	9.972472	LS	. . .	MP	
n046511	025846	S742000671	14:25:39.12	−88:14:54.1	13.77	0.14	0.07	9.618211	LS	788.7800	PR	
n047552	026640	S3YB000429	11:17:00.40	−88:35:36.4	9.37	0.38	10.24	. . .	. . .	. . .	LT	A
n047660	026730	S3YB000202	09:58:36.02	−88:23:59.9	12.89	0.11	0.13	2.066699	LS	786.2584	ED	
n049496	028221	S3YB000436	11:04:06.48	−88:38:02.5	13.55	0.25	0.38	4.815779	LS	788.6982	PR	
n050944	029379	S74E000029	15:57:05.68	−87:30:05.4	11.93	0.15	0.99	1.553117	LS	. . .	MP	A
n052190	030353	S3YA000615	08:39:40.45	−88:03:19.4	12.87	0.09	0.15	1.048425	LS	785.9799	PR	
n052325	. . .	S74E000072	15:44:44.17	−87:46:35.4	8.35	0.09	5.76	. . .	. . .	. . .	IR	
n054284	032007	S3YB000225	09:29:39.14	−88:30:06.4	11.78	0.12	0.98	0.621863	LS	785.5950	RL	A,G
n054942	032544	S3Y8000312	11:48:09.42	−88:49:52.6	10.39	0.05	1.27	25.795462	LS	. . .	MP	
n055150	. . .	S3YB000458	10:04:40.34	−88:40:25.5	9.06	0.04	1.41	0.092508	LS	785.2723	PR	
n057617	034669	S743000094	13:50:03.38	−88:46:13.2	10.08	0.06	1.40	15.167192	LS	. . .	MP	
n057725	034724	S3YB000482	10:01:18.94	−88:44:36.8	10.08	0.10	2.34	43.205800	LS	. . .	MP	A
n057789	. . .	S3Y8000318	11:19:13.27	−88:53:40.8	12.74	0.10	0.19	1.862438	LS	. . .	MP	
n058002	034997	S743000311	14:29:04.38	−88:38:43.7	12.13	0.61	5.88	0.646577	LS	785.6753	RL	A
n058442	. . .	S3YB000199	08:53:45.85	−88:26:33.0	12.41	0.07	0.21	0.258295	LS	785.2335	PR	
n058656	035468	S3YA000613	08:08:46.28	−88:00:02.0	13.86	0.17	0.09	0.822773	BLS	786.0050	ED	
n059543	036162	S3YB000243	09:03:59.29	−88:33:07.6	11.40	0.20	1.18	0.873857	LS	785.2020	ES	A
n060041	036526	S743000153	15:35:01.14	−88:16:11.9	13.16	0.95	4.98	. . .	. . .	. . .	LT	
n060566	036939	S743000200	15:25:11.74	−88:23:14.9	12.82	0.05	0.05	7.376734	LS	785.7479	PR	
n060667	037016	S743000186	15:28:41.36	−88:21:44.0	13.63	0.15	0.10	0.157962	LS	785.3571	PR	
n060789	. . .	S741000025	15:59:17.54	−88:00:42.5	14.23	0.26	0.03	6.853790	LS	789.0467	ED	
n062144	038255	S743000115	13:53:18.49	−88:54:14.6	12.87	0.47	2.17	0.266903	LS	785.2292	EC	A
n062519	038580	S3Y8000346	10:50:11.96	−88:59:54.1	11.78	0.05	0.21	5.745575	LS	787.1325	PR	
n062640	038663	S3YB000253	08:46:12.64	−88:33:42.9	12.00	0.44	5.22	0.267127	LS	785.2565	EC	A
n062696	. . .	S741000340	16:07:56.96	−87:59:09.7	11.98	0.08	0.31	1.185502	LS	785.2992	PR	
n062884	. . .	S740000057	12:30:49.10	−89:02:45.7	11.94	0.03	0.06	25.125450	LS	787.7145	PR	
n063743	039541	S740000060	12:36:24.67	−89:04:02.7	10.97	0.04	0.46	25.161758	LS	. . .	MP	
n064731	040351	S3YA000660	08:02:26.52	−88:14:26.1	13.34	0.11	0.13	0.285606	LS	785.4430	PR	
n065137	. . .	S74E000575	16:31:36.82	−87:40:07.7	12.11	0.09	0.27	5.388951	LS	790.4191	ED	
n066680	. . .	S3YL000291	07:14:42.32	−87:22:25.0	11.37	0.07	0.49	. . .	. . .	. . .	IR	
n066932	. . .	S743000330	15:21:39.34	−88:41:59.3	13.00	0.06	0.07	20.753202	LS	785.2020	PR	
n068660	043618	S3YB009826	08:40:28.89	−88:47:00.4	13.72	0.33	0.26	13.024607	LS	794.0587	ES	
n069025	043885	S3YB000275	08:17:16.96	−88:37:29.5	14.00	0.17	0.09	9.386448	LS	785.9529	PR	
n070113	044751	S740000101	13:01:29.04	−89:13:47.0	13.21	0.11	0.14	6.422671	LS	787.0902	PR	
n073013	047176	S3YA000181	07:12:14.54	−87:51:19.7	12.81	0.15	0.42	2.643748	LS	786.7776	PR	
n076289	. . .	S3YA000320	07:07:52.74	−88:02:11.4	12.94	0.10	0.13	0.789882	LS	785.4483	PR	
n076976	050375	S3YB013754	07:39:17.11	−88:40:41.7	13.46	0.10	0.06	1.441150	LS	785.6660	PR	
n077512	050773	S74E000469	17:10:42.44	−87:30:09.3	10.52	0.06	1.12	3.292027	LS	. . .	MP	
n078642	. . .	S3Y8000239	08:51:51.07	−89:15:21.3	12.27	0.05	0.09	3.481819	LS	785.5641	PR	

TABLE 3 — *Continued*

ID 2010	ID 2008	GSC	R.A. (J2000.0)[1]	Dec. (J2000.0)[1]	i (mag)	Δi_{90} (mag)	J	Period (d)	Src[2]	T_0^3 (d)	Class[4]	Note[5]
n080090	052891	S741000155	17:13:18.69	−87:42:28.6	9.44	0.17	8.41	59.365516	LS	. . .	MP	A
n080626	053446	S743000493	16:37:09.46	−88:43:24.2	11.29	0.04	0.23	35.753464	LS	. . .	MP	
n080649	. . .	S3YA000502	07:01:38.41	−88:17:02.9	9.60	0.05	1.52	23.466222	LS	. . .	MP	
n080770	053446	S3Y8000220	08:05:03.24	−89:07:54.3	12.95	0.13	0.20	1.071988	LS	786.1217	PR	
n080929	053570	S743000460	16:44:10.40	−88:38:19.9	11.02	0.03	0.26	19.967817	LS	. . .	MP	
n081202	053783	S3Y8000272	09:44:14.75	−89:28:17.6	10.48	0.02	0.18	16.047868	LS	. . .	MP	
n083000	. . .	S3Y8007194	09:23:04.69	−89:29:38.8	13.77	0.23	0.25	0.124657	LS	785.2675	PR	
n083359	055495	S3Y8000078	07:43:54.49	−89:07:37.3	12.52	0.39	1.45	0.797910	LS	785.8882	EC	A
n084427	055854	S3Y8000109	07:54:37.65	−89:15:40.9	9.75	0.08	1.67	. . .	. . .	. . .	IR	
n085632	057344	S741000539	17:13:42.52	−88:24:52.5	11.09	0.09	1.60	20.106163	LS	. . .	MP	
n086263	057775	S3YA000492	06:40:47.15	−88:15:21.3	11.73	0.39	4.71	0.438659	LS	785.4511	EC	A
n088489	. . .	S3YA016263	06:31:32.66	−88:11:38.1	12.81	0.09	0.13	0.240723	LS	785.4360	PR	
n088653	059811	S3YA000336	06:28:42.76	−88:02:41.7	12.35	0.12	0.23	7.254001	LS	787.3637	ED	
n090586	061353	S740000342	17:15:45.51	−89:00:42.8	10.78	0.02	0.18	0.022641	LS	785.2130	PR	
n090919	061658	S741000489	17:36:45.98	−88:14:10.5	11.31	0.03	0.24	0.076166	LS	785.2522	PR	
n091083	061740	S740000322	17:23:25.05	−88:53:37.3	9.99	0.07	2.20	34.479083	LS	. . .	MP	
n091084	061783	S740000308	17:25:37.17	−88:49:50.3	13.83	0.35	0.35	0.188993	LS	785.3176	DS	
n092211	062683	S3Y8000165	07:46:18.25	−89:40:00.7	10.27	0.04	0.75	15.857866	LS	. . .	MP	
n094368	064380	S3YA000248	06:10:28.12	−87:53:32.9	14.20	0.24	0.03	2.307363	LS	785.2020	PR	
n095083	064944	S741000460	17:51:13.16	−88:09:48.8	10.65	0.05	0.96	30.763139	LS	. . .	MP	
n095145	065072	S740000301	17:47:26.35	−88:46:07.9	11.87	0.05	0.18	0.620534	LS	785.6897	PR	
n096554	066196	S740000469	17:05:16.14	−89:51:43.8	9.67	0.04	1.06	26.623757	LS	. . .	MP	
n097049	. . .	S740012990	17:55:19.53	−89:07:43.2	14.97	0.56	0.14	0.348088	LS	785.2424	PR	
n097333	066775	S741000378	17:59:00.73	−88:01:32.9	11.76	0.18	1.86	38.853950	LS	. . .	MP	
n099251	068276	SA9S000144	18:22:33.29	−89:36:22.9	11.39	0.03	0.20	2.835357	LS	786.8351	PR	
n099286	068308	S0SG000353	05:50:34.20	−89:06:46.2	12.94	0.08	0.10	0.798947	LS	785.3570	PR	
n100083	068908	SA9U000383	18:08:15.09	−88:18:02.9	10.83	0.03	0.33	2.842765	LS	. . .	MP	
n101873	. . .	S0SH000511	05:43:48.57	−88:32:56.9	12.75	0.12	0.22	0.646457	LS	785.3882	PR	
n102304	070680	SA9S000413	22:05:02.55	−89:52:06.7	13.05	0.21	0.56	1.988474	LS	787.1308	ES	
n102641	070941	S0SH000225	05:47:08.05	−87:51:00.2	10.23	0.05	1.21	0.606546	LS	785.4046	GD	
n103401	071571	S0SH000333	05:43:19.93	−88:04:04.3	10.65	0.32	6.76	. . .	. . .	. . .	LT	A
n104524	072350	SA9V000050	18:30:57.87	−88:43:17.5	9.86	0.04	0.57	9.925551	BLS	788.2407	TR	
n104943	072730	SA9U000438	18:29:03.93	−88:32:31.9	13.32	0.51	1.85	0.573044	LS	785.7601	RL	A
n105244	. . .	S0SG000150	00:20:19.58	−89:48:38.0	9.43	0.04	1.22	10.923423	LS	. . .	MP	
n108372	. . .	SA9S000233	20:34:48.30	−89:34:03.2	12.81	0.07	0.12	2.371811	LS	785.4818	PR	
n109325	076135	SA9S000115	19:53:21.15	−89:22:46.5	10.37	0.33	8.00	. . .	. . .	. . .	IR	
n110028	076723	SA9V000063	19:00:22.60	−88:47:53.7	10.88	0.21	4.41	. . .	. . .	. . .	IR	
n110665	077190	S0SH000448	05:15:49.62	−88:17:51.5	10.21	0.04	0.92	11.462763	LS	. . .	MP	
n111158	077508	SA9S000404	22:53:06.46	−89:38:40.9	14.07	0.36	0.09	0.133318	LS	785.3185	PR	
n111246	077594	SA9V000067	19:08:12.87	−88:49:18.5	10.06	0.02	0.48	1.679604	LS	785.5144	PR	
n112440	078549	S0SH000321	05:15:49.03	−88:04:23.5	13.12	0.16	0.42	5.389812	LS	787.9077	PR	
n112694	078773	SA9V000073	19:17:53.08	−88:51:11.2	11.81	0.09	0.68	0.372068	LS	785.2474	EC	
n113158	. . .	SA9S000043	19:33:21.70	−89:00:22.9	8.67	0.17	2.29	. . .	. . .	. . .	IR	A
n113486	079397	SA9S000068	19:48:57.10	−89:07:14.3	10.86	0.02	0.21	4.842585	LS	788.1947	PR	
n114115	. . .	S0SG000229	03:01:17.31	−89:24:30.2	12.38	0.05	0.08	5.767268	BLS	785.6845	TR	
n115348	080934	SA9U000331	18:58:35.51	−88:12:55.2	11.72	0.24	2.83	62.185489	LS	. . .	MP	
n116034	. . .	S0SH000139	05:12:14.90	−87:44:42.1	8.43	0.13	8.84	. . .	. . .	. . .	IR	A
n116344	081723	SA9U000071	18:48:23.75	−87:43:16.4	11.49	0.07	0.67	0.841671	LS	785.5572	GD	
n116380	081749	. . .	19:11:53.61	−88:27:14.9	10.31	0.03	0.54	88.385466	LS	. . .	MP	
n116491	081845	SA9V000074	19:38:27.80	−88:50:51.9	12.90	0.10	0.09	6.759592	LS	785.3202	ED	
n116918	082180	S0SG000129	00:29:58.19	−89:30:20.3	11.24	0.02	0.15	0.152825	LS	785.3478	DS	
n117549	. . .	S0SG000213	02:55:59.73	−89:17:48.2	12.48	0.06	0.11	0.721620	LS	785.4964	PR	
n117763	. . .	SA9U000396	19:13:28.77	−88:21:56.0	12.84	0.12	0.27	0.151852	LS	785.2020	DS	
n118098	083110	S0SG000226	02:11:02.80	−89:22:50.3	10.27	0.03	0.43	6.623027	LS	. . .	MP	
n118528	. . .	SA9S000384	23:35:11.99	−89:27:51.8	14.78	1.23	0.86	0.465790	LS	785.3995	RL	G
n118992	. . .	SA9S000200	21:24:11.87	−89:17:56.5	14.69	0.52	0.15	0.233625	LS	785.2898	DS	
n119729	084344	SA9S000371	23:01:30.03	−89:25:01.5	13.96	0.18	0.07	2.927708	BLS	786.0597	PR	
n121493	085719	S0SG000178	03:08:19.12	−89:06:32.2	12.20	0.06	0.18	17.205471	LS	. . .	MP	
n122451	086480	S0SJ000306	03:44:10.88	−88:52:09.5	11.19	0.03	0.22	21.496218	LS	. . .	MP	
n122836	. . .	SAA5000323	19:02:33.97	−87:35:30.2	8.86	0.07	2.42	. . .	. . .	. . .	IR	
n123187	087084	SA9S000168	20:57:31.47	−89:03:50.3	12.36	0.33	0.76	1.857642	LS	786.7030	ED	
n123522	. . .	SA9U000336	19:27:57.26	−88:13:26.2	8.80	0.32	17.60	. . .	. . .	. . .	IR	A
n123706	087501	S0SG000092	01:23:01.27	−89:17:09.4	13.60	0.20	0.12	0.193489	LS	785.3819	DS	
n123782	087548	S0SH000485	04:20:11.85	−88:25:03.5	12.63	0.12	0.61	0.197741	LS	785.2566	DS	
n124517	088142	S0SG000093	00:52:40.76	−89:17:32.4	13.84	0.38	0.41	0.292944	LS	785.3965	EC	
n126026	089391	SA9U000387	19:43:40.77	−88:19:20.7	13.49	0.08	0.04	0.136874	LS	785.3534	PR	
n128266	. . .	S0SJ000248	03:37:18.58	−88:38:51.4	9.47	0.04	0.95	7.957924	LS	. . .	MP	
n130449	. . .	S0SG000064	00:24:32.27	−89:08:48.5	12.69	0.08	0.16	4.314518	LS	789.0505	PR	
n131494	093873	SA9S000300	22:17:44.44	−89:01:38.1	9.45	0.10	4.05	. . .	. . .	. . .	IR	
n132580	094793	S0SU000407	04:36:31.02	−87:28:03.3	10.97	0.09	1.50	0.617076	LS	785.5155	PR	
n132830	. . .	S0SH031178	04:00:54.92	−88:09:59.6	14.40	0.25	-0.00	0.159051	BLS	785.2264	PR	
n133214	. . .	S0SJ000325	02:03:09.66	−88:55:31.4	12.04	0.04	0.13	0.444790	LS	785.3150	PR	
n134610	096404	SAA5000420	19:43:05.07	−87:46:52.4	14.13	0.81	1.38	0.581666	LS	785.3416	RL	A
n134728	. . .	S0SJ014770	03:14:01.11	−88:32:53.1	14.42	0.39	0.07	1.209346	LS	785.8792	ED	
n135670	097230	SA9U000295	20:02:18.84	−88:02:50.0	12.08	0.10	0.21	9.548319	LS	789.9965	ED	

TABLE 3 — *Continued*

2010	ID 2008	GSC	R.A. (J2000.0)[1]	Dec.	i (mag)	Δi_{90}	J	Period (d)	Src[2]	T_0^3 (d)	Class[4]	Note[5]
n136750	098092	S0SH000022	03:54:41.13	−88:02:50.6	11.61	0.16	2.12	74.090207	LS	. . .	MP	A
n137559	098719	SAA5000417	19:50:26.13	−87:44:50.7	12.86	0.25	1.07	0.416436	LS	785.3327	EC	
n138555	099529	S0SG000018	00:31:15.83	−88:55:17.9	10.80	0.03	0.27	9.422044	LS	. . .	MP	
n140799	. . .	S0SJ016907	02:29:57.18	−88:34:35.3	14.32	0.22	-0.01	2.852904	LS	787.3254	PR	
n142023	. . .	S0SH031869	03:31:30.30	−88:04:24.4	14.45	0.34	0.07	0.722102	LS	785.7695	ES	
n142074	. . .	SA9V000177	21:19:45.21	−88:28:17.7	13.39	0.16	0.21	43.638939	LS	. . .	MP	
n142981	. . .	S0SJ000161	02:41:54.21	−88:26:02.9	10.98	0.04	0.47	11.204593	LS	. . .	MP	
n145245	. . .	S0SJ000052	00:56:07.00	−88:42:17.9	11.36	0.04	0.25	7.994425	LS	. . .	MP	
n145960	. . .	S0SJ000031	01:51:34.69	−88:33:26.9	12.01	0.06	0.27	10.882430	LS	. . .	MP	
n148233	107478	SAA5000503	20:28:30.07	−87:46:16.5	11.81	0.17	0.89	2.192580	LS	786.0746	ED	
n148619	. . .	SA9V011956	22:28:21.41	−88:31:41.0	14.34	0.22	0.01	3.817432	LS	788.6046	PR	
n149414	. . .	S0SJ000002	03:00:33.53	−88:02:59.2	10.13	0.86	29.50	. . .	. . .	. . .	LT	A,G
n150808	. . .	SA9T000439	23:03:39.20	−88:32:14.0	10.34	0.10	2.92	. . .	. . .	. . .	IR	A
n152437	110801	S0SI000269	02:42:27.87	−88:04:22.5	9.46	0.13	4.84	44.303305	LS	. . .	MP	A
n153006	111298	S0SI000438	02:12:56.05	−88:13:52.5	10.03	0.04	1.11	12.116866	LS	. . .	MP	
n156482	. . .	SA9T000422	23:57:27.17	−88:24:54.5	12.44	0.06	0.11	6.198528	LS	788.5551	ED	
n157627	. . .	S0SV000431	03:10:59.88	−87:35:38.1	10.61	0.08	1.16	. . .	. . .	. . .	IR	
n159243	. . .	S0SI000372	00:00:50.89	−88:19:41.9	9.44	0.04	1.12	0.114436	LS	785.2310	PR	
n160137	117654	S0ST000503	02:18:11.67	−87:56:11.2	10.57	0.09	1.68	22.012562	LS	. . .	MP	
n161425	118705	S0SI033411	00:53:26.68	−88:12:41.4	13.40	0.09	0.06	3.535402	BLS	786.7269	TR	
n162294	119488	S0SI000329	00:08:43.43	−88:13:48.4	10.07	0.11	3.59	. . .	. . .	. . .	IR	
n163148	120188	S0SI000289	00:55:45.92	−88:09:11.0	11.18	0.06	0.53	10.923423	LS	. . .	MP	
n163888	. . .	SA9T000268	22:46:01.56	−88:04:59.2	13.88	0.24	0.09	7.752665	LS	787.3176	ED	
n164527	121369	SA9T000310	23:15:35.46	−88:07:33.8	10.78	0.05	0.75	24.945468	LS	. . .	MP	
n167071	. . .	SAA6000049	21:52:26.36	−87:44:20.6	10.59	0.05	0.82	10.560170	LS	. . .	MP	
n167300	. . .	SAA7000327	21:12:08.31	−87:24:25.1	9.17	0.08	2.21	0.166200	LS	. . .	MP	
n167522	123934	SA9T000282	23:52:30.36	−88:03:49.5	13.94	0.14	0.04	0.122034	LS	785.2471	PR	
n167944	. . .	S0SV012740	02:52:25.60	−87:20:21.5	13.66	1.03	5.74	. . .	. . .	. . .	LT	
n168446	124666	SAA6000034	21:47:16.29	−87:39:06.6	12.84	0.62	3.88	0.458059	LS	785.5620	RL	A
n171256	. . .	SA9T000182	23:16:45.97	−87:54:16.6	11.95	0.07	0.29	8.754028	LS	. . .	MP	
n172241	127850	S0SI014387	00:00:52.46	−87:54:27.3	11.38	2.91	61.18	. . .	. . .	. . .	LT	G
n173163	. . .	SAA6000447	22:12:01.66	−87:37:04.2	9.57	0.07	2.75	. . .	. . .	. . .	IR	
n176396	. . .	SAA6000418	22:17:33.93	−87:31:44.4	10.71	0.06	0.79	. . .	. . .	. . .	IR	
n177534	131919	S0SI000101	00:01:16.84	−87:44:02.9	11.99	0.09	0.24	9.458450	LS	791.1664	ED	
n180169	133742	SAA6000366	22:37:07.30	−87:28:49.9	11.62	0.49	3.59	0.848393	LS	785.5973	EC	A
n181332	. . .	SA9T000064	23:30:39.10	−87:35:14.8	8.63	0.10	4.51	. . .	. . .	. . .	IR	A
n805954	005954	S742000078	12:39:58.23	−87:41:37.2	9.78	0.07	2.49	. . .	. . .	. . .	IR	
n863059	063059	S3Y8000125	06:49:54.20	−89:21:58.8	9.51	0.05	2.01	. . .	. . .	. . .	IR	
n897790	097790	SA9V000415	22:23:40.80	−88:53:42.9	9.77	0.03	0.78	0.521773	LS	785.6966	GD	

NOTE. — [1]: from GSC2.3 except for #n116380 (based on CSTAR master image) [2]: [LS], Lomb-Scargle method; [BLS], box-fitting algorithm. [3]: Epoch of primary eclipse or minimum light in JD-2454500. [4]: Classes: [DS]: δ Scuti; [EC/ED/ES]: eclipsing binary (contact, detached, semi-detached); [GD]: γ Doradus; [IR]: irregular; [LT]: long-term variation; [MP]: multi-periodic; [PR]: unclassified periodic; [RL]: RR Lyrae; [TR]: transit-like eclipse; [5]: [A]: in ASAS catalog; [G]: in GCVS.

previous surveys. For example, our observations reach $i \sim 15.3$ mag while the previous study of this area of the sky by ASAS reached a limiting magnitude of $V \sim 14.5$ mag (equivalent to $i \sim 13-14.5$ mag depending on spectral type). We recovered 35 of the 46 previously-known variables in our field; 5 were saturated, 3 were strongly blended and 3 did not meet our minimum requirement for synoptic coverage.

Our observations found significant variability or periodicity for 2.1% of the stars in the sample. This variable star fraction is in good agreement with the expectation for a survey like ours with a photometric precision limit of ~ 0.02 mag (see Fig. 9 of Tonry et al. 2005). Among the 44 variables selected by the analysis of §4.1, which did not discriminate by type of variability, 11% are strictly periodic (eclipsing binaries, RR Lyraes, etc.) while an additional 25% exhibit multi-periodic behavior and the the remaining 64% have no significant periodicity.

Table 4 lists statistics for the different types of objects we detected based on both searches (§4.1 and §4.2). The variable types are consistent with expectations for a red-sensitive survey directed towards a halo field. For example, nearly half of all variables exhibit low-amplitude/multi-periodic or long-term/irregular pulsations typical of RGB or AGB stars. 90% of the variables of these types present in our sample have $i < 12$ mag, and according to the Besançon model of the Galaxy (Robin et al. 2003) post-main sequence stars dominate the stellar population of our field in that magnitude range. The regular pulsators that we have been able to classify based on light curve shape or period are also post-main sequence or Population II objects, such as RR Lyrae or δ Scuti stars. In contrast, the eclipsing binaries and unclassified periodic variables have a broader distribution in magnitude, as expected for a mix of evolved and main sequence objects.

TABLE 4
DISTRIBUTION OF VARIABLE STAR TYPES

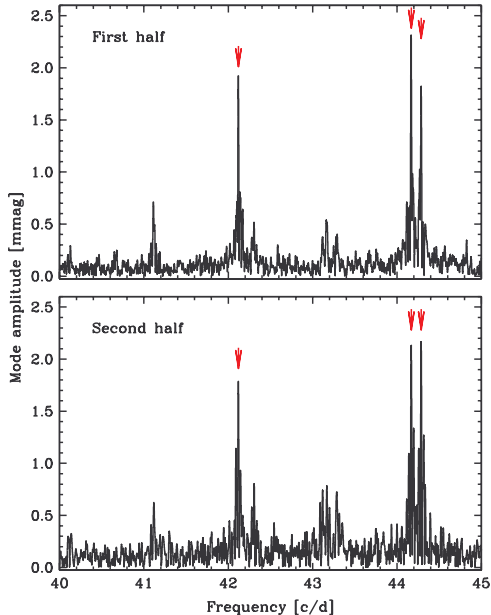| Variable Type	N	%
Multi-periodic	57	30.3
Unclassified periodic	47	25.0
Eclipsing binaries	35	18.6
Irregular/long-term	28	14.9
δ Sct	8	4.3
RR Lyr	7	3.7
γ Dor	3	1.6
Transit-like	3	1.6

FIG. 9.— Fourier spectrum of CSTAR #n090586 derived using the Period04 program, based on data obtained during the first (top) and second (bottom) half of the 2010 season. Three significant peaks (at $f_i = 44.288$, 44.169, and 42.121 cycles d^{-1}) are detected with varying amplitudes, which exhibit significant changes ($4-11\sigma$) relative to the 2008 season. See text for details.

FIG. 10.— Light curve of CSTAR#n057725, showing the slow reduction in Cepheid-like pulsation amplitude during the 2008 season has been replaced by a more complex variability in 2010. Eclipse-like events seem to be present at two distinct phases indicated with red and blue arrows, respectively.

We combined the two years of CSTAR photometry (from the 2008 and 2010 Antarctic winters) to search for changes in the observed properties of the variables. The very fast periodic variable #n090586 exhibited the same three significant frequencies first seen in the 2008 observations (see Fig. 17 of Wang et al. 2011), but the amplitude of each component exhibited significant temporal variations relative to the that season (at the -3.8, 7.8 and 11.4σ level, respectively). A comparison of the first and two halves of the 2010 data (Fig. 9) also shows a significant (-3.9σ) variation for one of the frequencies. We plan further research on this object using a fast-pulsating stellar model.

The 2010 light curve of CSTAR#n057725 ($P = 43.2$ d), originally discovered by the ASAS project (Pojmanski 2005) and classified as a fundamental-mode δ Cephei variable, showed a dramatic change relative to 2008 as seen in Fig. 10. The Cepheid-like variability seen in the 2008 data (top-left panel), which already showed indications of a change in amplitude, decreased even further and developed a secondary peak in the 2010 data (top-right panel). Furthermore, eclipse-like events can now be seen at two distinct phases of the pulsation (bottom panels) separated by half of the period with depths of ~ 0.07 and ~ 0.03 mag. The V-band ASAS light curve, spanning more than a decade, also shows secular variations in pulsation amplitude. The ASAS classification of this object is very unlikely; at $i = 10.1$ mag, a 43-day Cepheid would lie ~ 17 kpc away and nearly 8 kpc above the Galactic plane, an extremely improbable location for an $\sim 11 M_\odot$ star. It is more likely that this object consists of a Population II pulsator, such as an RV Tauri or the Galactic equivalent of an OGLE small-amplitude variable red giant (Soszynski et al. 2004) in a
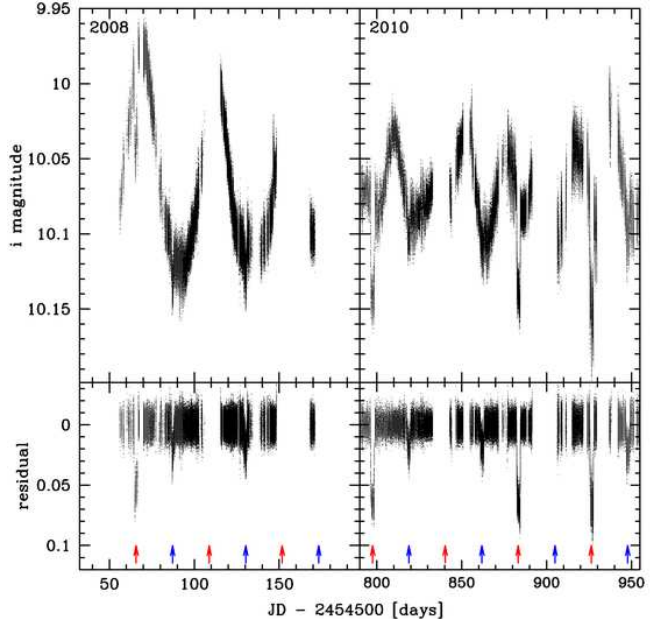
binary system. We plan to undertake additional observations to investigate the nature of this system.

5. CONCLUSIONS AND SUMMARY

We have presented the analysis of high-cadence synoptic observations of 23 square degrees centered on the south celestial pole, conducted with the CSTAR#3 telescope at Dome A during 183 days of the 2010 Antarctic winter season. 86% of all frames obtained at a sun elevation angle below 0° yielded useful data. We measured a median sky background of 19.8 mag /□″ over all moon phases and determined that the extinction is below 0.1 mag for 40% of the time (0.4 mag for 70% of the time). All these values are consistent with the site statistics derived from the 2008 season, and reinforce the promise of the Antarctic Plateau for future astronomical work.

We carried out time-series aperture photometry of 9,125 stars with $i < 15.3$ mag. We detected 188 variable stars, including 67 new objects not included in our previous work thanks to a slightly larger field of view and a deeper magnitude limit. This represents a $\sim 4\times$ increase in the number of variable stars relative to previous surveys of the same region of the sky. We plan follow-up multi-wavelength photometry and high-resolution spectroscopy in the near future of the most interesting variables, such as detached eclipsing binaries and the candidate transiting exoplanets.

Given the coarse pixel scale of our images and our use of aperture photometry, the search for (non-periodic) variable stars was limited to objects with low levels of crowding. This could mitigated by the use of difference imaging techniques in future analyses. The apparent circular motion of stars in the field of view, due to the fixed

nature of the telescope and camera, prevented the detection of periodic variability at frequencies close to one sidereal day (and its harmonics) despite the absence of a day/night cycle and the long duration of the observations. Future surveys conducted from Antarctica would greatly benefit from instruments with improved angular resolution, a finer pixel scale, and the ability to track. The recently-deployed AST3 telescopes (Cui et al. 2008) meets all these criteria and should greatly expand our synoptic capabilities in the polar regions.

Facility: Dome A: CSTAR

REFERENCES

Ashley, M. C. B., Allen, G., Bonner, C. S., Bradley, S. G., Cui, X., Everett, J. R., Feng, L., Gong, X., Hengst, S., Hu, J., Jiang, Z., Kulesa, C. A., Lawrence, J. S., Li, Y., Luong-Van, D. M., McCaughrean, M. J., Moore, A. M., Pennypacker, C., Qin, W., Riddle, R., Shang, Z., Storey, J. W. V., Sun, B., Suntzeff, N., Tothill, N. F. H., Travouillon, T., Walker, C. K., Wang, L., Yan, J., Yang, H., York, D. G., Yuan, X., Zhang, X., Zhang, Z., Zhou, X., & Zhu, Z. 2010, Highlights of Astronomy, 15, 627

Burton, M. G. 2010, A&A Rev., 18, 417

Charbonneau, D., Brown, T. M., Latham, D. W., & Mayor, M. 2000, ApJ, 529, L45

Cui, X., Yuan, X., & Gong, X. 2008, in Society of Photo-Optical Instrumentation Engineers (SPIE) Conference Series, Vol. 7012, Society of Photo-Optical Instrumentation Engineers (SPIE) Conference Series

Hartman, J. D., Gaudi, B. S., Holman, M. J., McLeod, B. A., Stanek, K. Z., Barranco, J. A., Pinsonneault, M. H., & Kalirai, J. S. 2008, ApJ, 675, 1254

Hengst, S., Allen, G. R., Ashley, M. C. B., Everett, J. R., Lawrence, J. S., Luong-Van, D. M., & Storey, J. W. V. 2008, in Presented at the Society of Photo-Optical Instrumentation Engineers (SPIE) Conference, Vol. 7012, Society of Photo-Optical Instrumentation Engineers (SPIE) Conference Series

Henry, G. W., Fekel, F. C., Henry, S. M., & Hall, D. S. 2000, ApJS, 130, 201

Howell, S. B. 2012, PASP, 124, 263

Kaluzny, J., Stanek, K. Z., Krockenberger, M., Sasselov, D. D., Tonry, J. L., & Mateo, M. 1998, AJ, 115, 1016

Kenyon, S. L., Lawrence, J. S., Ashley, M. C. B., Storey, J. W. V., Tokovinin, A., & Fossat, E. 2006, PASP, 118, 924

Kovács, G., Zucker, S., & Mazeh, T. 2002, A&A, 391, 369

Lawrence, J. S., Allen, G. R., Ashley, M. C. B., Bonner, C., Bradley, S., Cui, X., Everett, J. R., Feng, L., Gong, X., Hengst, S., Hu, J., Jiang, Z., Kulesa, C. A., Li, Y., Luong-Van, D., Moore, A. M., Pennypacker, C., Qin, W., Riddle, R., Shang, Z., Storey, J. W. V., Sun, B., Suntzeff, N., Tothill, N. F. H., Travouillon, T., Walker, C. K., Wang, L., Yan, J., Yang, J., Yang, H., York, D., Yuan, X., Zhang, X. G., Zhang, Z., Zhou, X., & Zhu, Z. 2008, in Presented at the Society of Photo-Optical Instrumentation Engineers (SPIE) Conference, Vol. 7012, Society of Photo-Optical Instrumentation Engineers (SPIE) Conference Series

Lawrence, J. S., Ashley, M. C. B., Burton, M. G., Cui, X., Everett, J. R., Indermuehle, B. T., Kenyon, S. L., Luong-Van, D., Moore, A. M., Storey, J. W. V., Tokovinin, A., Travouillon, T., Pennypacker, C., Wang, L., & York, D. 2006, in Presented at the Society of Photo-Optical Instrumentation Engineers (SPIE) Conference, Vol. 6267, Society of Photo-Optical Instrumentation Engineers (SPIE) Conference Series

Lawrence, J. S., Ashley, M. C. B., Hengst, S., Luong-Van, D. M., Storey, J. W. V., Yang, H., Zhou, X., & Zhu, Z. 2009, Rev Sci Instrum, 80, 064501

Lenz, P. & Breger, M. 2005, Communications in Asteroseismology, 146, 53

Lomb, N. R. 1976, Ap&SS, 39, 447

Luong-Van, D. M., Ashley, M. C. B., Cui, X., Everett, J. R., Feng, L., Gong, X., Hengst, S., Lawrence, J. S., Storey, J. W. V., Wang, L., Yang, H., Yang, J., Zhou, X., & Zhu, Z. 2010, in Presented at the Society of Photo-Optical Instrumentation Engineers (SPIE) Conference, Vol. 7733, Society of Photo-Optical Instrumentation Engineers (SPIE) Conference Series

Mosser, B. & Aristidi, E. 2007, PASP, 119, 127

Nugent, P. E., Sullivan, M., Cenko, S. B., Thomas, R. C., Kasen, D., Howell, D. A., Bersier, D., Bloom, J. S., Kulkarni, S. R., Kandrashoff, M. T., Filippenko, A. V., Silverman, J. M., Marcy, G. W., Howard, A. W., Isaacson, H. T., Maguire, K., Suzuki, N., Tarlton, J. E., Pan, Y.-C., Bildsten, L., Fulton, B. J., Parrent, J. T., Sand, D., Podsiadlowski, P., Bianco, F. B., Dilday, B., Graham, M. L., Lyman, J., James, P., Kasliwal, M. M., Law, N. M., Quimby, R. M., Hook, I. M., Walker, E. S., Mazzali, P., Pian, E., Ofek, E. O., Gal-Yam, A., & Poznanski, D. 2011, Nature, 480, 344

Ofek, E. O. 2008, PASP, 120, 1128

Pojmanski, G. 2005, VizieR On-line Data Catalog: J/other/AcA/50.177. Originally published in: Acta Astronomica, 50, 177 (2001)

Robin, A. C., Reylé, C., Derrière, S., & Picaud, S. 2003, A&A, 409, 523

Samus, N. N., Durlevich, O. V., & et al. 2009, VizieR Online Data Catalog, 10, 2025

Saunders, W., Lawrence, J. S., Storey, J. W. V., Ashley, M. C. B., Kato, S., Minnis, P., Winker, D. M., Liu, G., & Kulesa, C. 2009, PASP, 121, 976

Saunders, W., Lawrence, J. S., Storey, J. W. V., Ashley, M. C. B., Kato, S., Minnis, P., Winker, D. M., Liu, G., & Kulesa, C. 2010, in EAS Publications Series, Vol. 40, EAS Publications Series, ed. L. Spinoglio & N. Epchtein, 89–96

Scargle, J. D. 1982, ApJ, 263, 835

Schlafly, E. F. & Finkbeiner, D. P. 2011, ApJ, 737, 103

Soszynski, I., Udalski, A., Kubiak, M., Szymanski, M., Pietrzynski, G., Zebrun, K., Szewczyk, O., & Wyrzykowski, L. 2004, Acta Astronomica, 54, 129

Stellingwerf, R. F. 1978, ApJ, 224, 953

Stellingwerf, R. F. 2011, in RR Lyrae Stars, Metal-Poor Stars, and the Galaxy, ed. A. McWilliam, 47

Stetson, P. B. 1987, PASP, 99, 191

—. 1996, PASP, 108, 851

Storey, J. W. 2009, Assoc Asia Pac Phys Soc Bull, 19, 4

Storey, J. W. V. 2005, Antarctic Science, 17, 555

—. 2007, Chinese Astron. Astrophys., 31, 98

Tonry, J. L., Howell, S. B., Everett, M. E., Rodney, S. A., Willman, M., & VanOutryve, C. 2005, PASP, 117, 281

Udalski, A., Szymanski, M., Stanek, K. Z., Kaluzny, J., Kubiak, M., Mateo, M., Krzeminski, W., Paczynski, B., & Venkat, R. 1994, Acta Astronomica, 44, 165

Wang, L., Macri, L. M., Krisciunas, K., Wang, L., Ashley, M. C. B., Cui, X., Feng, L.-L., Gong, X., Lawrence, J. S., Liu, Q., Luong-Van, D., Pennypacker, C. R., Shang, Z., Storey, J. W. V., Yang, H., Yang, J., Yuan, X., York, D. G., Zhou, X., Zhu, Z., & Zhu, Z. 2011, AJ, 142, 155

Yang, H., Allen, G., Ashley, M. C. B., Bonner, C. S., Bradley, S., Cui, X., Everett, J. R., Feng, L., Gong, X., Hengst, S., Hu, J., Jiang, Z., Kulesa, C. A., Lawrence, J. S., Li, Y., Luong-Van, D., McCaughrean, M. J., Moore, A. M., Pennypacker, C., Qin, W., Riddle, R., Shang, Z., Storey, J. W. V., Sun, B., Suntzeff, N., Tothill, N. F. H., Travouillon, T., Walker, C. K., Wang, L., Yan, J., Yang, J., York, D., Yuan, X., Zhang, X., Zhang, Z., Zhou, X., & Zhu, Z. 2009, PASP, 121, 174

Young, A. T. 1967, AJ, 72, 747

Yuan, X., Cui, X., Liu, G., Zhai, F., Gong, X., Zhang, R., Xia, L., Hu, J., Lawrence, J. S., Yan, J., Storey, J. W. V., Wang, L., Feng, L., Ashley, M. C. B., Zhou, X., Jiang, Z., & Zhu, Z. 2008, in Society of Photo-Optical Instrumentation Engineers (SPIE) Conference Series, Vol. 7012, Society of Photo-Optical Instrumentation Engineers (SPIE) Conference Series

Zhou, X., Fan, Z., Jiang, Z., Ashley, M. C. B., Cui, X., Feng, L., Gong, X., Hu, J., Kulesa, C. A., Lawrence, J. S., Liu, G., Luong-Van, D. M., Ma, J., Moore, A. M., Qin, W., Shang, Z., Storey, J. W. V., Sun, B., Travouillon, T., Walker, C. K., Wang, J., Wang, L., Wu, J., Wu, Z., Xia, L., Yan, J., Yang, J., Yang, H., Yuan, X., York, D., Zhang, Z., & Zhu, Z. 2010a, PASP, 122, 347

Zhou, X., Wu, Z., Jiang, Z., Cui, X., Feng, L., Gong, X., Hu, J., Li, Q., Liu, G., Ma, J., Wang, J., Wang, L., Wu, J., Xia, L., Yan, J., Yuan, X., Zhai, F., Zhang, R., & Zhu, Z. 2010b, Research in Astronomy and Astrophysics, 10, 279

Zou, H., Zhou, X., Jiang, Z., Ashley, M. C. B., Cui, X., Feng, L., Gong, X., Hu, J., Kulesa, C. A., Lawrence, J. S., Liu, G., Luong-Van, D. M., Ma, J., Moore, A. M., Pennypacker, C. R., Qin, W., Shang, Z., Storey, J. W. V., Sun, B., Travouillon, T., Walker, C. K., Wang, J., Wang, L., Wu, J., Wu, Z., Xia, L., Yan, J., Yang, J., Yang, H., Yao, Y., Yuan, X., York, D. G., Zhang, Z., & Zhu, Z. 2010, AJ, 140, 602